

# **A method of improving viewing resolution for the three-dimensional integral imaging by use of moving array-lenslet technique**

동적 배열렌즈 기법을 사용하여 완전 결  
상의 관측을 향상시키는 방법



A thesis submitted in partial fulfillment of the requirements

for the degree of Master of Engineering

in the Department of Telematics, Graduate School,

Pukyong National University

February 2005

# 조명진의 공학석사 학위논문을 인준함

2005년 2월 25일

주 심 공학박사 정 신 일



위 원 공학박사 김 성 운



위 원 공학박사 하 덕 호



(인)

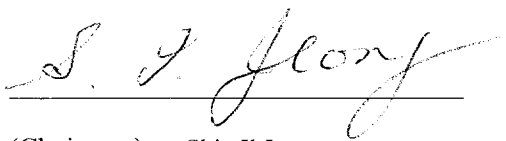
**A method of improving viewing resolution for the three-  
dimensional integral imaging by use of moving array-lenslet  
technique**

**A Dissertation**

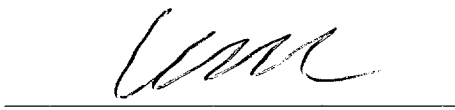
**by**

**Myungjin Cho**

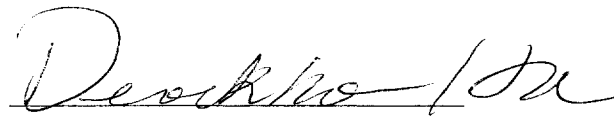
Approved as to style and content by :



(Chairman) Shin Il Jeong



(Member) Sung-Un Kim



(Member) Deock-Ho Ha

February, 2005

# CONTENTS

I. Introduction .....	1
II. Improvement of the viewing resolution using MALT .....	4
1. The review of integral imaging .....	4
2. The viewing resolution of integral imaging .....	6
3. Moving Array-Lenslet Technique (MALT) .....	7
III. Three-dimensional integral imaging of micro-objects using confocal scanning microscopy .....	11
1. Confocal microscopy .....	11
2. Computer synthesized integral imaging using confocal microscopy	12
IV. Improvement characteristics of viewing resolution according to moving path of lenslet array .....	17
1. Experimental method .....	17
2. Experimental result .....	23
V. Experiment for integral imaging using confocal microscopy	32
VI. Conclusion .....	36
References .....	37

## LIST OF FIGURES

Figure 1. Principle of 3-D integral imaging. (a) Pickup process using a pinhole lens array. In the direct pickup process, a lenslet array is used for high light efficiency. A pinhole lens array can be used when the pickup process is digitally synthesized to obtain elemental images according to ray optics. (b) Reconstruction of 3-D image using a lenslet array. ....	5
Figure 2. The moving direction of the lenslet array in MALT .....	9
Figure 3. Computer pickup for given sectioning images, and optical 3-D image reconstruction in space. The longitudinal position of the pinhole array is set at $z = 0$ . Observers are assumed to be positioned at $z > 0$ . (a) Pickup for real 3-D image display. Locations of sectioning images along the $z$ axis, $z_1, z_2, \dots, z_N$ , are positive values. (b) Pickup for virtual 3-D image display. Locations of sectioning images along the $z$	

axis, $z_1, z_2, \dots, z_N$ , are negative values. (c) Real 3-D image display. (d) Virtual 3-D image display.....	13
Figure 4. Sectioning image and elemental image used in experiments.....	16
Figure 5. (a) Objects used in experiments. (b) Calculation method for elemental images through computer synthesized. ....	18
Figure 6. Elemental images in the specific position of the lenslet array .....	21
Figure 7. Reconstructed 3-D image when MALT is not applied. ....	24
Figure 8. The example to apply MALT. (a) Linear moving path and sampling position. (b) Reconstructed 3-D image. ....	24
Figure 9. The example to apply MALT. (a) Diagonal moving path with tilting angle $45^\circ$ and sampling position. (b) Reconstructed 3-D image. (c) Diagonal moving path with tilting angle $18^\circ$ and sampling position. (d)	

Equivalent sampling path and position expressed in one pitch size of lenslet. (e) Reconstructed 3-D image. ....	26
Figure 10. The example to apply MALT. (a) Moving path and sampling position. (b) Reconstructed 3-D image. (c) Equivalent sampling path expressed in circular area with rotating radius $5p/4$ . (d) Reconstructed 3-D image. ....	29
Figure 11. The example to apply MALT. (a) Moving path and sampling position with uniform distribution. (b)-(f) Reconstructed 3-D images observed at various viewing points. ....	31
Figure 12. Synthesized elemental images. Only 8 sectioning images selected from a total of 26 sectioning images. ....	34
Figure 13. Reconstructed 3-D image displayed optically in space. As the viewing direction changes, the perspective varies continuously. ....	35

Figure 14. Reconstructed 3-D image displayed optically in space using MALT. As the viewing direction changes, the perspective varies continuously..... 35



# 동적 배열렌즈 기법을 사용하여 완전 결상의 관측 해상도를 향상시키는 방법

조 명 진

부경대학교 대학원 정보통신공학과

## 요 약

3 차원 완전 결상에서 동적 배열 렌즈 방식을 사용하여 관측 해상도를 향상시킬 때, 해상도 향상 특성을 조사하였다. 렌즈 배열의 이동 방향 및 이동 거리에 따라 관측 해상도가 달라짐을 컴퓨터 합성 완전 결상을 이용하여 보였다. 이를 통해 효율적으로 관측 해상도를 향상시킬 수 있는 렌즈 배열의 이동 조건을 찾을 수 있다. 또한, 3 차원 완전 결상을 사용하여 공간상에 미세 물체를 디스플레이하는 방법을 제안한다. 여기서, 요소 영상은 공초점 마이크로스코피를 사용하여 서로 다른 깊이를 따라 광학적으로 2 차원 샘플링을 통해 계산된다. 균일한 확대율을 가지는 3 차원 생물체를 공간상에 디스플레이할 수 있고 그로 인해 완전 결상이 공초점 마이크로스코피의 3 차원 디스플레이에 사용될 수 있음을 실험 결과를 통해 증명할 수 있다.

# **A method of improving viewing resolution for the three-dimensional integral imaging by use of moving array-lenslet technique**

**Myungjin Cho**

*Department of Telematics Engineering, Graduate School  
Pukyong National University*

## **Abstract**

We investigate characteristics of viewing resolution improvement in three-dimensional integral imaging, when a dynamic lens array method is adopted. We show that the viewing resolution changes for different moving directions and distances of the lens array through computer-synthesized integral imaging. From this study, optimal moving conditions of the lens array for efficient viewing resolution improvement can be determined. We also propose a method to display micro-objects in space based on three-dimensional integral imaging, in which elemental images are calculated from two-dimensional sampling of the optical field along different depth using confocal scanning microscopy. Experimental results are presented to demonstrate that a uniformly magnified three-dimensional biological specimen can be displayed in space and thus integral imaging can be used for three-dimensional display of confocal microscopy.

# **I. Introduction**

The study for three-dimensional (3-D) display has been researched for a long time based on the holography or the stereoscopy method [1-3]. Although holography is regarded as ideal 3-D display method, it needs a coherent light source and is difficult to record the object, which is far from the lenslet array, and reconstruct it. Stereoscopy method induces the 3-D effect as the observer sees two different 2-D images with binocular parallax through left and right eye. It is simple to realize and can display the 3-D images with high viewing resolution and large depth of focus by use of two planar images. However, stereoscopy has only horizontal parallax, which is difficult to display the 3-D images with full parallax. It has a visual fatigue because of convergence-accommodation conflict. Also, the viewing point is not continuous as it has the fixed viewing point or several ones.

Recently, the study for integral imaging (II) has been researched to avoid disadvantages of stereoscopy method. It was originally by the name of integral photography (IP) and first proposed by Lippmann in 1908 [4-6]. It is the method to implement the real-time integral photography by use of display panel and optical components such as a charge-coupled device (CCD) [7, 8]. It is advantages that II can display the 3-D images with both continuous viewing point and full parallax. But, there are many problems to limit practical applications, for example the narrow viewing angle, the

limited depth of focus, and the low viewing resolution [9-11]. To overcome these problems, several solutions have been proposed and experimented recently [12-17]. In our study, moving array-lenslet technique (MALT) has been proposed, which can improve the viewing resolution increasing the spatial sampling rate for the ray of lenslet array in time domain [12]. However, in previous work, there is not an investigation about relationship between detailed movements of lenslet array and improvement of the viewing resolution.

There has always been great interest in visualization of micro objects [18-21]. For both recording and display of the 3-D image of an object, lenslet elements with 1 or 2 mm aperture have been used [6]. However, it cannot be applied to micro-objects smaller than each micro-lens. The use of magnifying lenses before the pickup process cannot be a solution, because magnification is non-uniform along the longitudinal depth direction, and thus the 3-D shape cannot be preserved for a magnified image [22]. The use of a micro-lens array with lenslets much smaller than that of the micro-object is not a solution either, because diffraction in each micro-lens becomes significant and thus the image resolution is degraded seriously [11].

In this paper, we investigate characteristics of the viewing resolution improvement in 3-D integral imaging, when a dynamic lenslet array method is adopted. For this, we show that the viewing resolution changes for different moving directions and distances of the lenslet array through computer-synthesized integral imaging (CSII). From this study, optimal

moving conditions of the lenslet array for the efficient viewing resolution improvement can be determined.

We show that uniformly magnified 3-D images of micro-objects can be displayed in space using II. For this, we use uniformly magnified 2-D sectioning images of a 3-D micro-object along different depths, which are obtained from confocal scanning microscopy. The ray information for 3-D image formation is calculated from the sectioning images, and used in II to display 3-D micro-objects. Our approach can deal with semitransparent micro-object, such as microbiological cells.

## **II. Improvement of the viewing resolution using MALT**

### **1. The review of integral imaging**

Figure 1 is depicted principle of pickup and reconstruction in integral imaging. In general, the pinhole array is used to pickup and reconstruct but it is common that the lenslet array is used to improve the efficiency of light. Let us consider that 3-D object is as arbitrary distance as far from the lenslet (or pinhole) array. As depicted in Fig. 1(a), each lenslet (or pinhole) in lenslet (or pinhole) array records the direction and intensity information of rays coming from 3-D object by 2-D light detectors such as CCD. This ray information is equal to the small images for 3-D object and thus it is referred to as the elemental images. If 2-D display panel such as liquid crystal display (LCD) represents these elemental images and they are reconstructed through the same lenslet array for the pickup, a 3-D image is formed as rays are intercrossed in space, as depicted in Fig. 1(b). The real image formed in Fig. 1(b) is pseudoscopic. However, the orthoscopic virtual image can be obtained by rotating each elemental image as 180 degree central symmetrically or as using a lens the orthoscopic real image can be obtained [8, 23]. The elemental images are not obtained directly by lenslet array, but synthesized by the computer and thus these are called computer synthesized or generated integral imaging (CSII, CGII) [24].

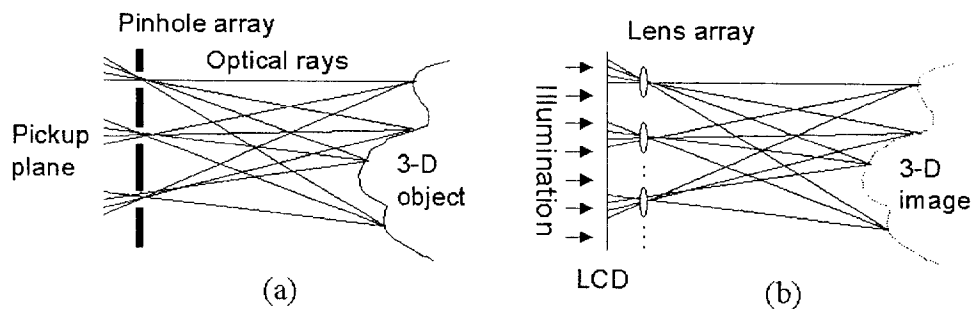


Figure 1. Principle of 3-D integral imaging. (a) Pickup process using a pinhole lens array. In the direct pickup process, a lenslet array is used for high light efficiency. A pinhole lens array can be used when the pickup process is digitally synthesized to obtain elemental images according to ray optics. (b) Reconstruction of 3-D image using a lenslet array.

## 2. The viewing resolution of integral imaging

In general the viewing resolution of the reconstructed 3-D image is determined by many system parameters, for example, the size and the pitch of lenslets and the resolution of the CCD and the display device. It is obvious that the number of pixels in the pickup and display devices is important in determining the 3-D image resolution, because all the elemental images should be detected and displayed with sufficient resolution. In II, however, one of the most fundamental factors that limit the viewing resolution of the reconstructed 3-D images is the pitch of the lenslet array, which determines the sampling rate of the elemental subimages in the spatial dimension. From the Nyquist sampling theorem, the upper limit of the viewing resolution in a lateral dimension is given by [9]

$$\beta_{nyq} \approx L/2p \quad (1)$$

in cycles per radian (cpr), where  $p$  is the pitch of the lenslet array in the lateral dimension and  $L$  is the distance between the observation point and the display lenslet array. However, if we reduce  $p$  (i.e., if the size of lenslet element is too small), diffraction of the lenslet limits the resolution even though the resolution of the detector and the display is infinite. Many authors have studied an optimal lenslet size, which is roughly 1 or 2 mm in reasonable viewing circumstances [6]. For example, suppose that  $p = 1$



mm and  $L = 0.5$  m (i.e.,  $\beta_{nyq} = 250$  cpr). This means that we cannot discern images whose size is less than  $\sim 2$  mm from a distance of 0.5 m. Such low resolution limits the usefulness of II in practical applications.

### 3. Moving Array-Lenslet Technique (MALT)

In the MALT, to increase the spatial sampling rate, the positions of the lenslet arrays for both pickup and display are rapidly vibrated synchronously in the lateral directions within the retention time of the afterimage (or, faster than the flicker fusion frequency) of the human eye. The vibration (or movement) range does not need to be larger than one pitch in both lattice directions, because the lenslet array is periodic. The elemental image detection device and the image display device are stationary. Because the pickup lenslet array and the display lenslet array vibrate synchronously, and human vision operates by averaging what it detects, observers see a stationary reconstructed image with improved viewing resolution for a stationary object. The price we have to pay for the improved viewing resolution in the MALT is that we have to use the image pickup and display devices that are fast enough to represent moving elemental images.

When the lenslets are packed in a square lattice with a pitch of  $p$ , 2-D motions are necessary to increase the spatial sampling rate along mutually orthogonal two-lattice directions in general. Because the lenslet array has

a periodic structure, however, even if the lenslet array moves only along the  $x$  axis with a velocity of  $V$ , we can increase the sampling rate along the two lattice direction ( $x'$  and  $y'$  directions) by tilting the lenslet array by  $\theta$ , where  $\theta$  is the angle between  $x$  and  $x'$ . This circumstance is depicted in Fig. 2. In this case, the velocity component of the lenslet array in the  $x'$  direction becomes  $V \cos \theta \equiv V_{x'}$ , while that in the  $y'$  direction becomes  $V \sin \theta \equiv V_{y'}$ . As the lenslet moves, the elemental images also move. Moving (i.e., time-varying) elemental images are detected (or sampled) by the 2-D image sensor and then displayed in the spatial light modulator (SLM) or LCD. The time-sampled elemental images should be integrated in the time domain in the observer's eyes without flickering. Because the lenslet array has a periodic structure, the elemental image pattern repeats in the time domain as the pickup lenslet array moves. For stationary objects, therefore,  $V_{x'}$  and  $V_{y'}$  should satisfy the following conditions:  $V_{x'} = V \cos \theta > pS$  and  $V_{y'} = V \sin \theta > pS$ , where  $S$  is the flicker fusion frequency of the human eye. When the objects to be imaged move with a maximum velocity of  $V_{\max}$ , the velocity of the lenslet array should be increased accordingly for time-domain integration without perceptual flickering in the eye. In general, the moving velocity of the lenslet array along the  $x$  direction should satisfy [14]

$$V > \max \left( \frac{pS}{\cos \theta} + V_{\max, x'}, \frac{pS}{\sin \theta} + V_{\max, y'} \right) \quad (2)$$

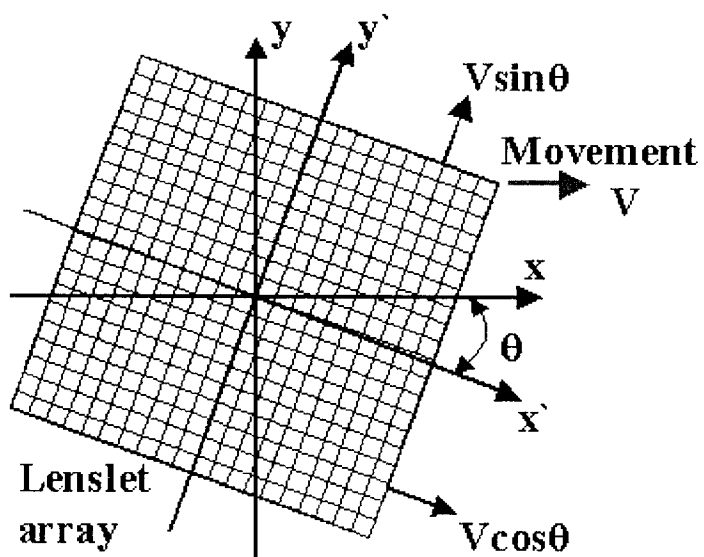


Figure 2. The moving direction of the lenslet array in MALT

where  $V_{\max,x'}$  and  $V_{\max,y'}$  are the velocity components of  $V_{\max}$  along  $x'$  and  $y'$  axes, respectively. For a stationary object, because  $S$  is approximately 50 Hz for human eyes, we get  $V > 70$  [mm/s] when  $\theta = 45^\circ$  and  $p = 1$  mm. Therefore the electronic shutter speed of the 2-D image sensor and the frame rate of the spatial light modulator (SLM) should be high enough to present the moving elemental images clearly.

In conventional TV and video systems, the frame rate is fixed typically at 60 Hz (or, two 30 Hz frames are interlaced). So there exists a limit for the display of a fast moving object clearly, because the time domain resolution is also limited by the Nyquist sampling rate in the time domain. In the MALT, the increase of the spatial sampling rate of ray information by lenslet is achieved in the time dimension. The object velocity is added to the moving velocity of the lenslet array according to Eq. (2). Therefore the frame rate of the 2-D image sensor and the SLM should be increased by a factor of  $\max(p/V_x, p/V_y)$  in the MALT to display the moving object with a similar time resolution of conventional TV and video systems.

### **III. Three-dimensional integral imaging of micro-objects using confocal scanning microscopy**

#### **1. Confocal microscopy**

To get 3-D images of micro-objects such as biological specimens, confocal (laser scanning) microscopy is widely used [3, 23]. In this technique, sharply focused light is illuminated on a 3-D specimen and reflected light (or fluorescent light, if the specimen is properly treated with dye) is detected. A 2-D image of a slice of the specimen centered in the focal plane (called a sectioning image) is obtained by scanning the specimen at that focal plane. A stack of sectioning images (and thus a volumetric image) is obtained by sweeping through the specimen along the optical axis (i.e., depth) direction. So far, there was no way to form a 3-D image of micro-objects with a 2-D display panel. The 3-D nature of the volumetric image is visualized by use of either computer simulation, sequential plane-by-plane display in time domain, or stereoscopic method that may produce visual fatigue.

## 2. Computer synthesized integral imaging using confocal microscopy

In our 3-D display approach, II is used to form a true 3-D image of a micro-object displayed in space. The image is a uniformly magnified version of the micro-objects in both lateral  $(x, y)$  and longitudinal  $(z)$  scales. The elemental images are calculated from a volumetric image with sufficient resolution obtained from for example, a confocal microscope. First, we assume that a sequence of images representing sections of the 3-D micro-object are positioned either in front of or behind a hypothetical pickup pinhole lens array, as depicted in Fig. 3(a) and (b). Then, considering the sequence of sectioning images as a volumetric image of the magnified micro-object, we synthesize elemental images by simulating the direct pickup process of an II system according to geometrical optics. When the calculated elemental images are displayed using a lenslet array and a 2-D display panel, observers will view either a real 3-D image or a virtual 3-D image in the same way the sectioning image are positioned as depicted in Fig. 3(c) and (d). The pitch (period) of the hypothetical pinhole array, denoted by  $p$ , should be equal to the pitch of the display lenslet array. The gap distance  $g$  should be properly selected for optimal focusing of the displayed 3-D image for a given focal length of lenslets  $f$ . If the distance between the lenslet (or pinhole lens) array and the central sectioning image is  $L$ ,  $g$  should be  $Lf/(L+f)$  for virtual image display, and  $Lf/(L-f)$  for real image display according to the Gauss lens law.

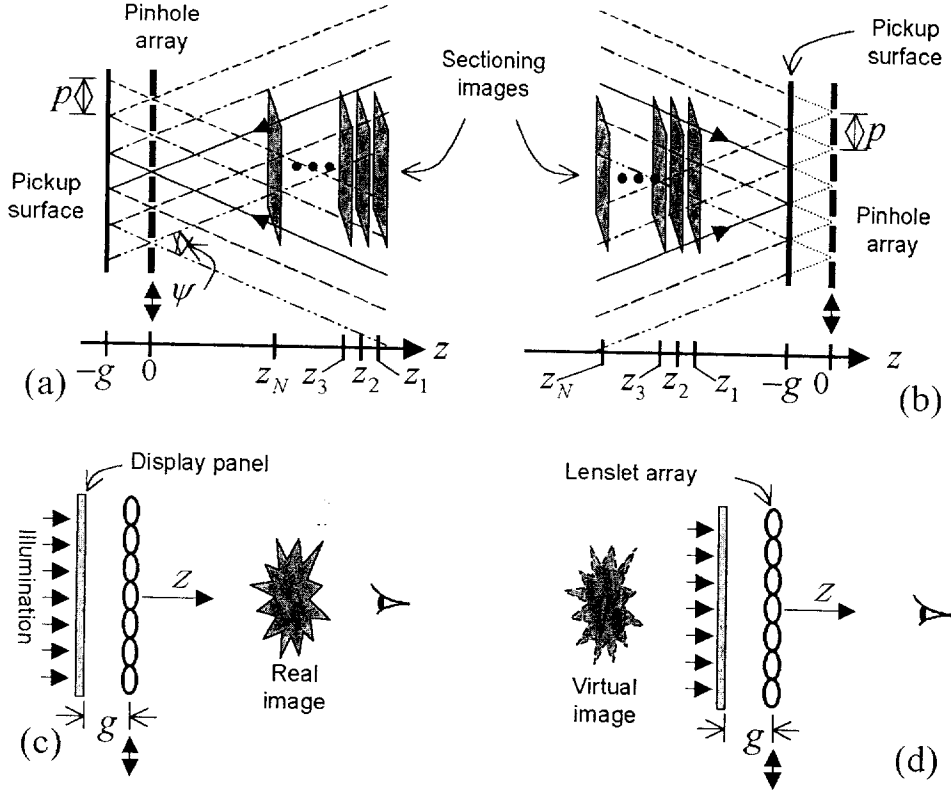


Figure 3. Computer pickup for given sectioning images, and optical 3-D image reconstruction in space. The longitudinal position of the pinhole array is set at  $z = 0$ . Observers are assumed to be positioned at  $z > 0$ . (a) Pickup for real 3-D image display. Locations of sectioning images along the  $z$  axis,  $z_1, z_2, \dots, z_N$ , are positive values. (b) Pickup for virtual 3-D image display. Locations of sectioning images along the  $z$  axis,  $z_1, z_2, \dots, z_N$ , are negative values. (c) Real 3-D image display. (d) Virtual 3-D image display.

The light intensity distributions of sectioning images located at  $z > 0$  should be mapped through corresponding pinholes into the pickup surface, and those in  $z < 0$  should be mapped directly into the pickup surface [25]. If the light intensity distribution of the  $k$ th sectioning image subtended by an angle of  $\psi$  for the  $i$ th pinhole is given by  $V_C(x_i, y_i, z = z_k)$ , where subscript  $C = 1$  (for red), 2 (for green) and 3 (for blue), the light intensity distribution of the corresponding pickup surface  $S_C(x_i, y_i, z = -g)$  becomes

$$S_C(x_i, y_i, -g) = \frac{1}{M(x_i, y_i)} \sum_{k=1}^N A_C(k) \cdot V_C(\beta_k x_i, \beta_k y_i, z_k) \quad (3)$$

where  $x_i$  and  $y_i$  are the local coordinates for the  $i$ th pinhole that positions at  $x_i = y_i = 0$ , and  $N$  is the number of sectioning images.  $M(x_i, y_i)$  is a normalization factor, which is the number of times the pixel values are added at position  $(x_i, y_i)$ .  $A_C(k)$  is introduced to take into account light absorption inside the semitransparent micro-object. Therefore, backward sectioning images will suffer from more absorption than front sectioning images. The scaling factor  $\beta_k$  is given by  $-z_k/g$ , where the minus sign indicates inverted image mapping through the pinhole lens.

To avoid interference between the neighboring elemental images at the pickup surface, we set  $\psi = 2 \arctan(p/2g)$ . The viewing angle of the 3-D reconstructed images is also limited by  $\psi$  [8, 14]



To demonstrate our approach experimentally, we used 26 color sectioning images of grape stamen tetrads which are the four cell products of meiosis in the male reproductive structure (stamen) of grape [26]. Each sectioning image has resolution of 512×512 pixels. A few of samples and the synthesized elemental image are shown in Fig. 4. For simplicity, we assume that there is uniform absorption inside the specimen,

$$A_C(k) = \begin{cases} \exp(-\alpha k), & \text{if } \sum_{C=1}^3 \sum_{m=0}^{k-1} V_C(\beta_m x_i, \beta_m y_i, z_m) \neq 0 \text{ and } k > 1; \\ 1, & \text{otherwise,} \end{cases} \quad (4)$$

where  $\alpha$  is a positive number.  $\alpha = 0$  implies a transparent object and  $\alpha = \infty$  implies an opaque object.

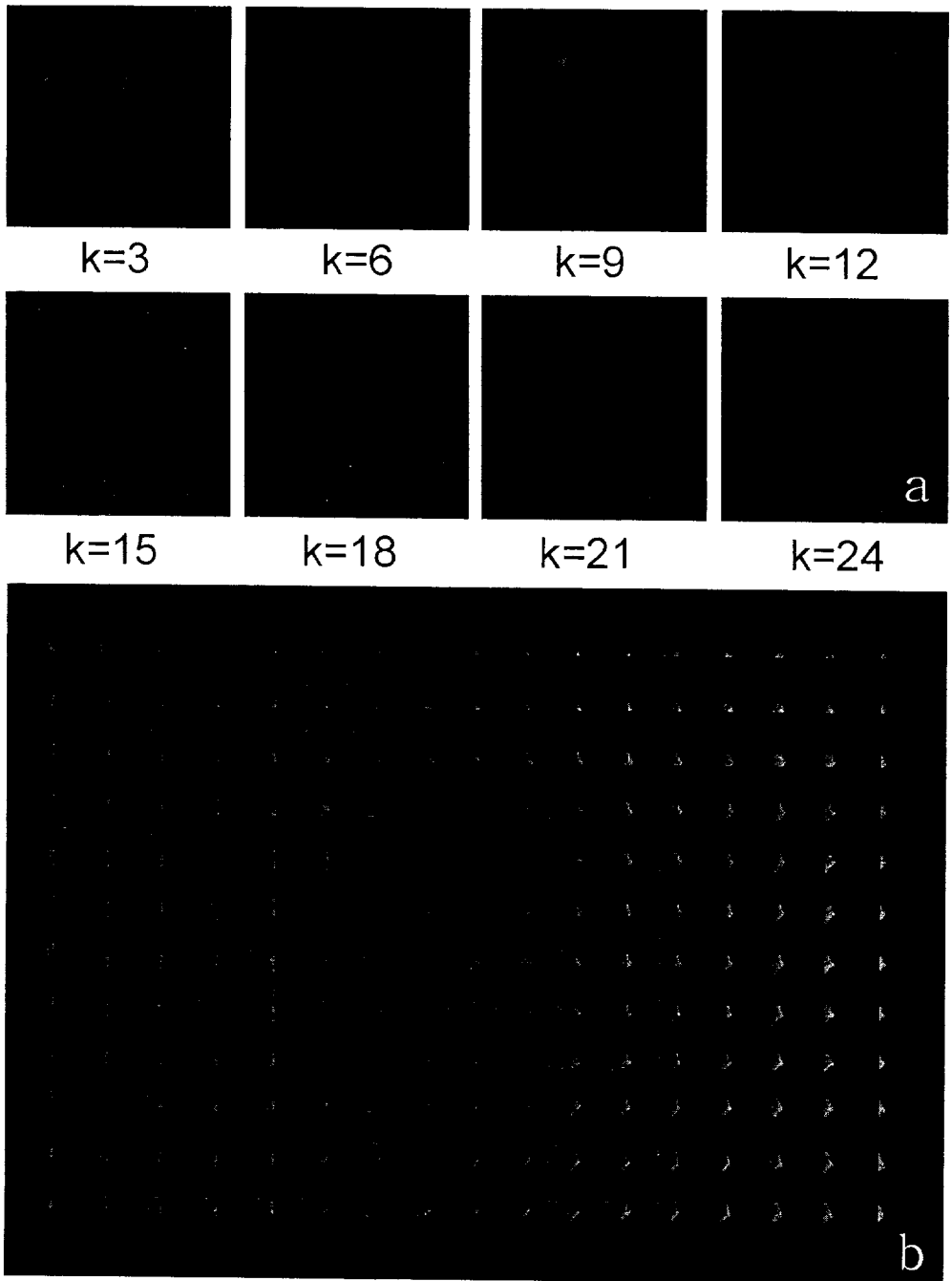


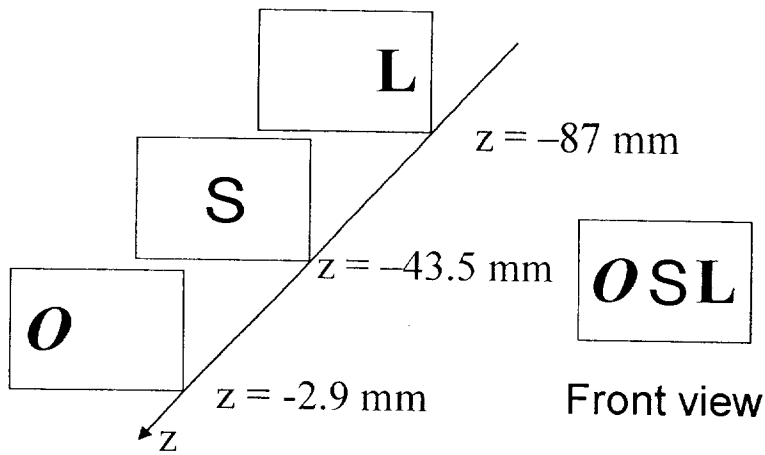
Figure 4. Sectioning image and elemental image used in experiments.

## **IV. Improvement characteristics of viewing resolution according to moving path of lenslet array**

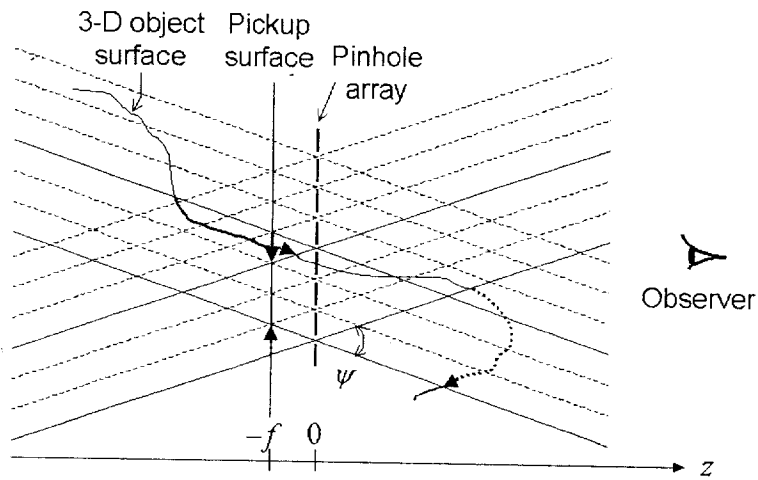
### **1. Experimental method**

In this experiment, lenslet array has  $53 \times 53$  square-shaped lenslet of which focal length is approximately 2.9 mm and the pitch is 1.08 mm. Each lenslet is separated less than  $7 \mu\text{m}$ . To display the elemental images, we used the penetration-type monochromatic LCD panel. The uniform based size of pixel in panel is  $36 \mu\text{m}$  and resolution is  $1024 \times 768$ .

The objects to display are O, S, and L. As depicted in Fig. 5(a), these three characters are displayed at each position 2.9 mm, 43.5 mm, and 87 mm from display lenslet array. The size of every character is approximately  $18 \text{ mm} \times 18 \text{ mm}$ . The distance between lenslet array and display panel is fixed as the focal length of lenslet array. To simplify the experiment, we did not use direct pickup but computer synthesized integral imaging.



(a)



(b)

Figure 5. (a) Objects used in experiments. (b) Calculation method for elemental images through computer synthesized.

The method to calculate the elemental images is depicted in Fig. 5(b). The hypothetical pinhole array with the same pitch of display lenslet array is set and then hypothetical pickup plane (or the position at which the panel to display the elemental image is located) is set at  $z = -g$ . 3-D objects are positioned at displayed plane. Virtual rays coming from the 3-D objects are mapped in pickup plane through pinhole. If the displayed image is the virtual image (i.e., the image positioned at  $z < 0$ ), demagnified images are mapped in pickup plane directly without rotating. Unless above, rotated images are existed because rays are mapped through pinhole. Pickup angle  $\psi$  for the 3-D objects of each pinhole is determined by pitch of pinhole and distance  $g$  between the pinhole and pickup plane. Therefore, the mapping area of objects' surface as roughly  $pD/g$  is varied by how far objects' surface is from pinhole array. Here,  $p$  is the pitch of pinhole,  $D$  is the distance between 3-D object and pinhole array, and  $g$  that is the distance between pinhole array and pickup plane is set the same focal length of lenslet array. If the overlapping part between forward displayed object and backward displayed object is existed, backward object must be hidden by forward object. So, when the several objects are picked up, we consider the overlapping part using the method to overwrite the pickup results for the closest plane from observer's eyes in order as using the pickup image of from farthest to closest one from observer's eyes. The mapped rays density is adjusted to corresponding to the number of pixels on display plane.

As the rays are mapped through all pinhole by this method, we can obtain the total elemental images. Fig. 6 is the elemental image for three characters pattern, O, S, and L, when lenslet array is fixed. The number of lenslet array used in the experiment is  $34 \times 25$  lenslets, because the resolution of LCD is fixed as  $1024 \times 768$  and the resolution of the elemental images for each lenslet is  $30 \times 30$  pixels. Therefore, Since the total resolution of the elemental image is  $1020 \times 750$  pixels and should be the same as the resolution of LCD, we add blanks.

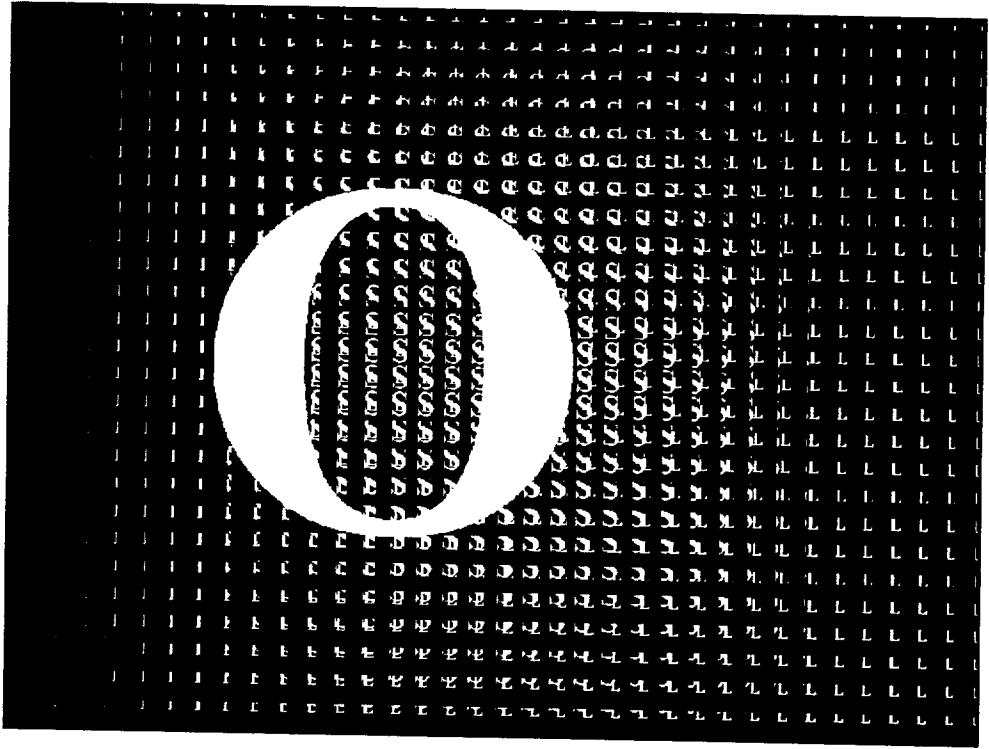


Figure 6. Elemental images in the specific position of the lenslet array

The method applying the moving array-lenslet technique is followed. First, the display lenslet array (pinhole array for the pickup) determines moving path in the  $x-y$  plane. The pickup plane and 3-D objects are fixed, the position of pinhole is moved in the  $x-y$  plane through moving path, and then the above pickup procedure is repeated. Each elemental image for these processes is similar to Fig. 6, but the detailed image of each one has some differences. These elemental images are stored in the computer. When the 3-D images are reconstructed, the display lenslet array also moves through the same path of  $x-y$  plane. As the lenslet array is moved at a particular position, corresponding elemental image is displayed. In other words, the correct elemental image synthesized through the moving path of the display lenslet array is represented in the display panel. At the moment, the lenslet array is moved and the elemental image is represented by sufficiently fast velocity as expressed in Eq. (2) because displayed 3-D image has to be seen continuously to the observer's eyes. However, we implemented the simulation of the afterimage effect that the reconstructed 3-D image is recorded by CCD camera and is averaged out by computer because the velocity of the device used in our experiment is very slow. The focal length of the lens used in CCD camera is 50 mm and the aperture size is 3 mm ( $f/\# = 16$ ). The resolution is increased, because the larger aperture size the more increased sampling bandwidth of ray information by lenslet array [12]. However, in the MALT, we implemented our experiment minimizing the aperture size to represent the effect of the resolution improvement well.



The moving path types are linear, circular, and so on in the  $x-y$  plane for applying the MALT. Especially, in the case of linear moving, we implemented our experiment changing the lattice direction, the moving direction, the tilting angle, and moving distance of the lenslet array.

## 2. Experimental result

If the elemental image in Fig. 6 is displayed through the display lenslet array, we can obtain the 3-D image with the low viewing resolution as depicted in Fig. 7. The viewing resolution is determined by the same spatial sampling period as the pitch of lenslet array.

If the lenslet array is moved to vertical direction (the direction of  $y$  axis or  $\theta = 90^\circ$  direction), the viewing resolution is improved for the only one axis. As the total lenslet array is moved, the same movement is occurred in each lenslet. Fig. 8(a) represents the moving path and the sampling position for the corresponding area as a lenslet size. As the pixel number of the corresponding elemental images for a lenslet is  $30 \times 30$ , these are also represented as a lattice. The position generating the ray sampling becomes the center of each lenslet. These sampling positions are marked as black spots. Because the sampling interval is quantized by the pixel size of the elemental image, the black square-shaped spot is made to be a pixel size in the display panel.

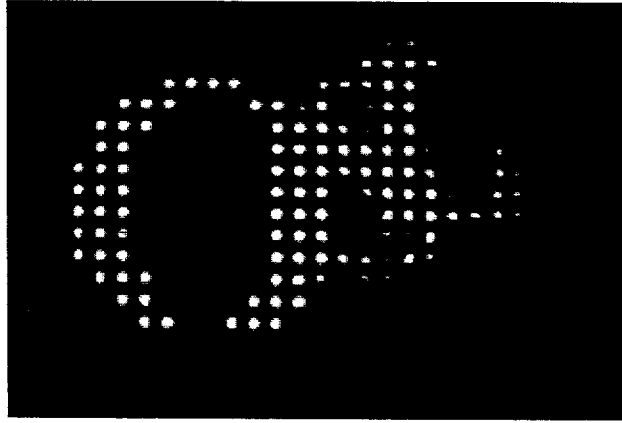
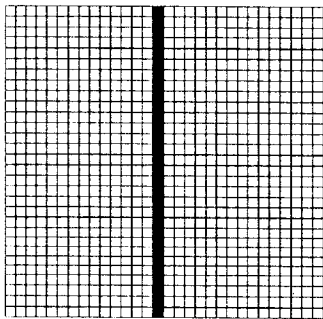
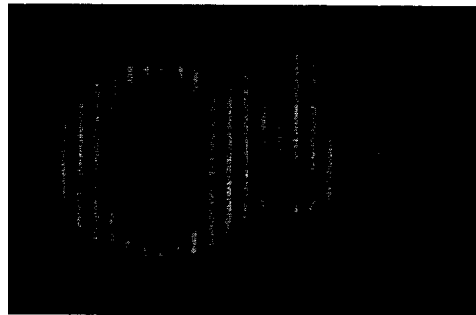


Figure 7. Reconstructed 3-D image when MALT is not applied.



(a)



(b)

Figure 8. The example to apply MALT. (a) Linear moving path and sampling position. (b) Reconstructed 3-D image.

To improve the viewing resolution of the direction of both  $x$  and  $y$  axis, we implemented our experiment by the moving direction of lenslet array with tilting angle. Fig. 9(a) represents the moving path and sampling position when tilting angle  $\theta$  is 45 degrees, Fig. 9(b) is the reconstructed image. The viewing resolution is improved toward the only diagonal direction, because sampling bandwidth is narrow and the ray sampling position is distributed non-uniformly in a space. These problems can be solved by the movement with  $\theta = 18^\circ$  ( $d = 3.16p$ ) as depicted in Fig. 9(c).

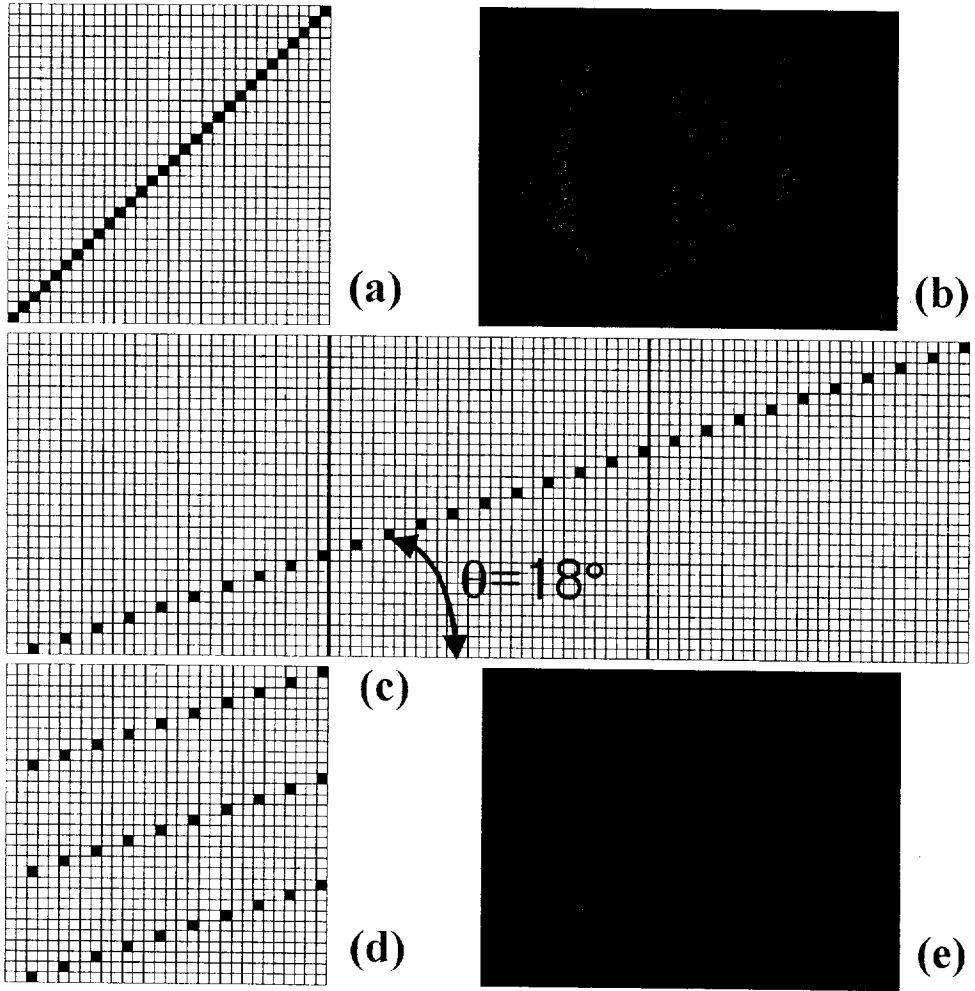


Figure 9. The example to apply MALT. (a) Diagonal moving path with tilting angle  $45^\circ$  and sampling position. (b) Reconstructed 3-D image. (c) Diagonal moving path with tilting angle  $18^\circ$  and sampling position. (d) Equivalent sampling path and position expressed in one pitch size of lenslet. (e) Reconstructed 3-D image.

Because lenslets are positioned periodically, if moving distance is more than a pitch, the sampling position can be overlapped by the neighboring lenslet. The moving path and the sampling position in Fig. 7(c) are equivalent to the ones in Fig. 7(d). In other words, in this case, the viewing resolution is improved because the sampling position is uniform for the area of a lenslet. The total sampling rate is 30 in our experiment. Fig. 9(e) is the reconstructed image. We can expect that the ray sampling positions have to be distributed uniformly and lenslet array has to be moved densely for the efficient resolution improvement. In general, the optimal moving condition that the sampling for each lenslet array is not overlapped spatially is given by following

$$\theta = \arctan(1/n); \quad d = p(1+n^2)^{1/2} \quad (3)$$

where  $n$  is the integer which represents the moving distance horizontally as a multiple of the lenslet pitch and  $\theta$  is the angle between the horizontal axis and the moving direction. In the previous MALT study, the circular movement had been proposed to simplify the implementation of system [12, 14]. In the case of moving the lenslet array mechanically, the linear movement with infinite moving distance of one direction cannot be done, and the movement of opposite direction is needed definitely. At the moment when the moving direction is changed, lenslet array stays and resolution is not improved. Therefore, the movement without stationary moment like the circular movement is better. However, in the circular

movement case, it is not good that rotating radius  $r$  is set the integer multiple of half pitch of the lenslet array. This is why the position of sampling cannot be distributed uniformly. To show this, we implemented the sampling process similar to the circular movement with rotating radius  $p/2$  as Fig. 10(a). In spite of 96 sampling points, the viewing resolution cannot be improved as depicted in Fig. 10(b). This is reason that the sampling points near outside line are redundant each other. To reduce the redundancies and sample uniformly in space, it is better that the rotating radius is selected by following.

$$r = np/2 + p/4 \quad (4)$$

where  $n$  is natural with zero, for example, Fig. 10(c) is in the case of  $n = 2$ . As a result, the viewing resolution is improved as depicted in Fig. 10(d).

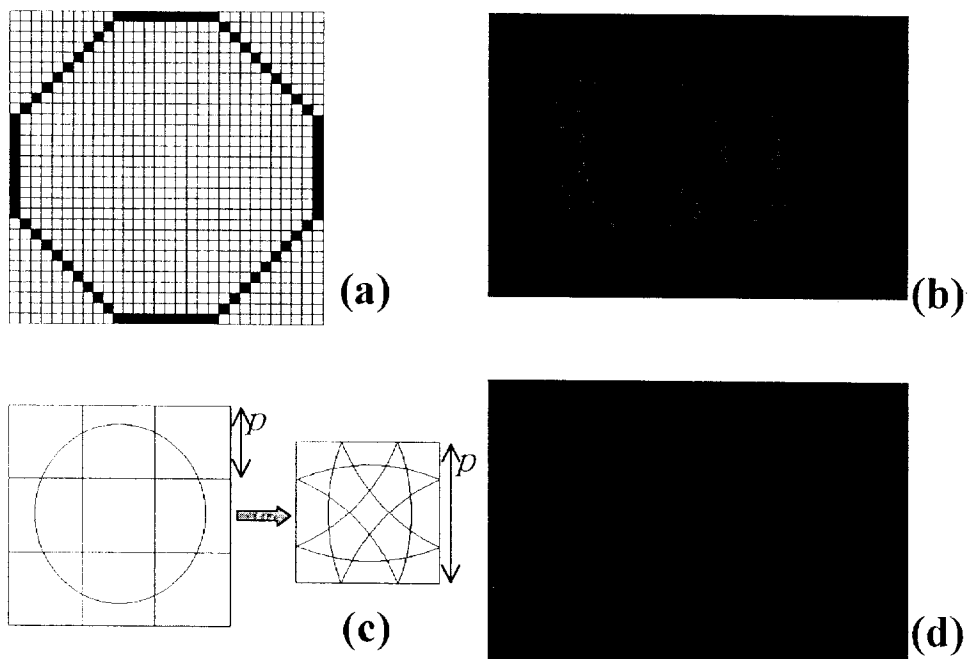


Figure 10. The example to apply MALT. (a) Moving path and sampling position. (b) Reconstructed 3-D image. (c) Equivalent sampling path expressed in circular area with rotating radius  $5p/4$ . (d) Reconstructed 3-D image.

Based on the previous experiment, Fig. 11(a) is the most ideal position of sampling. In fact, this is the type similar to Fig. 9(c) [or Fig. 9(e)]. This movement is the square-shaped spiral and zigzag. In this case, we analyze the properties of the viewing resolution improvement. The figures, which are observed at various viewing points when 36 sampling processes are implemented and the reconstructed images of each case are averaged depicted in Fig. 11(b)-(f). So we can know that the viewing resolution is improved efficiently only by the MALT and uniform sampling distribution. If lenslet array is synthesized and the movement is controlled electronically, the movement of lenslet array can be implemented variously [27]. In this case, the infinite linear movement of lenslet array can be implemented. To increase the sampling rate in the direction of  $x$  and  $y$  axis, lenslet array must be moved as the angle  $\theta$  is decreased and sampling process is implemented densely.



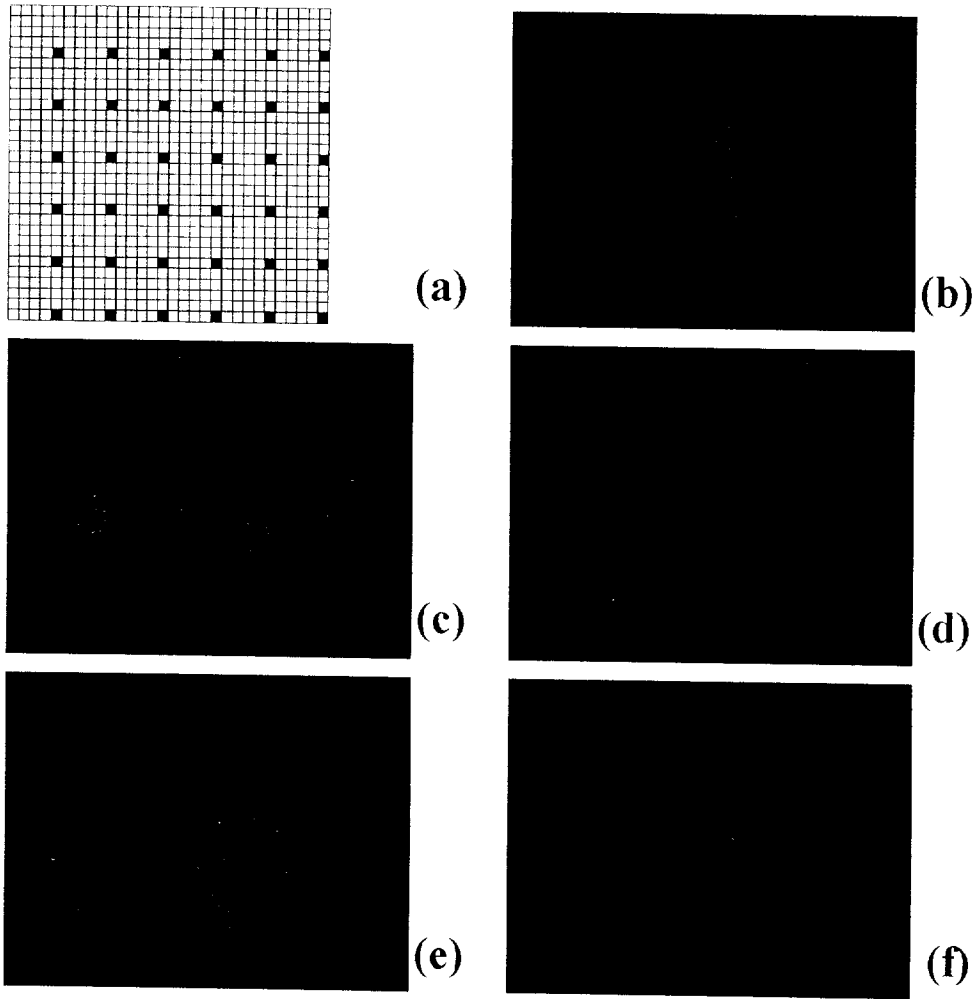


Figure 11. The example to apply MALT. (a) Moving path and sampling position with uniform distribution. (b)-(f) Reconstructed 3-D images observed at various viewing points.

## V. Experiment for integral imaging using confocal microscopy

We synthesized the elemental images for virtual 3-D image display. The elemental images for low absorption coefficient (e.g.,  $\alpha = 0.05$ ) are illustrated in Fig. 12, where the size of each sectioning image equals 9.2 mm. Because there are 26 sectioning images, the 3-D image depth of the displayed object is 26 mm. In fact, we exaggerated the image depth to emphasize that a uniformly magnified image through the depth direction is displayed. The display lenslet array has  $53 \times 53$  lenslets. Each lenslet is square-shaped and has a uniform base size of  $1.09 \times 1.09$  mm, with less than  $7.6 \mu\text{m}$  separating the lenslets. The focal length of the lenslets is approximately 3 mm and thus we set  $g = 2.5$  mm. We used an off-the-shelf LCD projector with three LCD panels for 3-D color image display. Each panel has  $1024 \times 768$  square pixels with a pixel pitch of  $18 \mu\text{m}$ .  $60 \times 60$  pixels were used to represent each elemental image. Thus, approximately  $17 \times 13$  lenslets (or elemental images) were used to display the sectioning images. The optically reconstructed 3-D image observed from three different directions are shown in Fig. 13. Each image was captured with a color CCD camera positioned at  $z \approx 20$  cm. As the observation direction changes, perspectives of the 3-D image displayed in space vary continuously, which demonstrates the 3-D nature of the displayed image. However, its viewing resolution is very low. So, we implemented the

experiment with MALT to improve the viewing resolution. The averaged reconstructed 3-D image observed from three different directions using MALT are shown in Fig. 14. From this, we can prove that the viewing resolution is improved by using MALT.

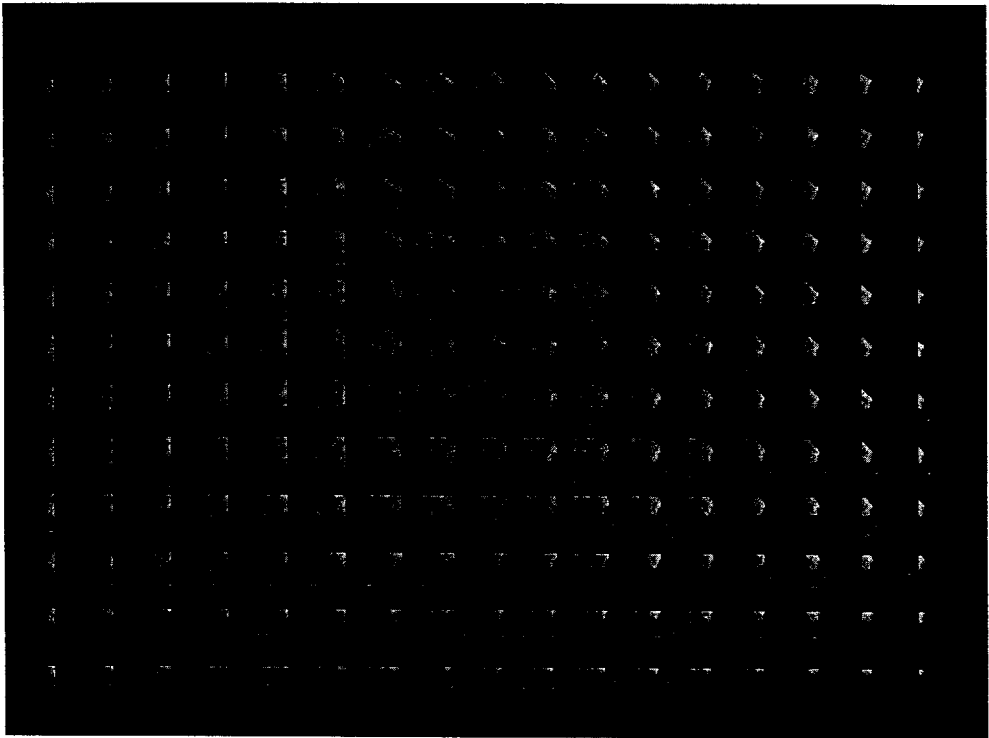


Figure 12. Synthesized elemental images. Only 8 sectioning images selected from a total of 26 sectioning images.

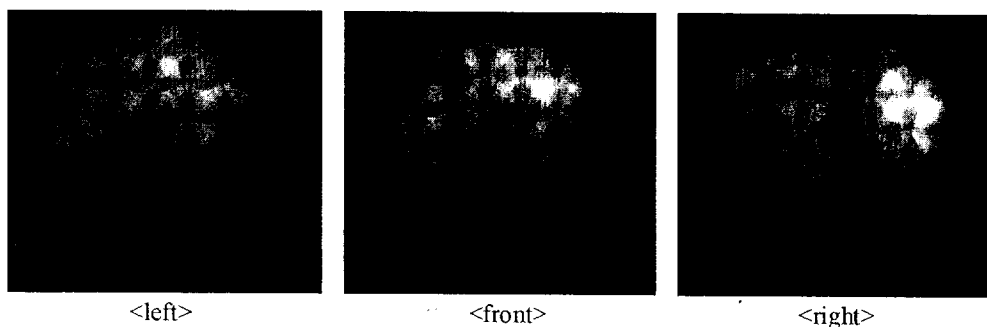


Figure 13. Reconstructed 3-D image displayed optically in space. As the viewing direction changes, the perspective varies continuously.

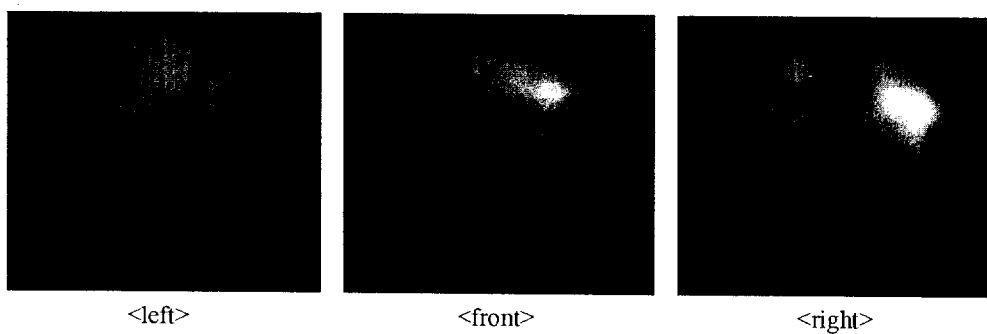


Figure 14. Reconstructed 3-D image displayed optically in space using MALT. As the viewing direction changes, the perspective varies continuously.

## VI. Conclusion

The viewing resolution, the viewing angle, and the depth-of-focus of 3-D integral images are limited in integral imaging [9, 11, 14]. These limitations can be relaxed by use of high-resolution display panels and a time multiplexing technique [9, 12, 14]. Application of our approach is not localized to microscopy. Sectioning images of other objects, for example, a volumetric image of the human body obtained from magnetic resonance imaging (MRI), can also be used to form and optically display a true 3-D image in space.

In conclusion, we have presented a new 3-D optical display method, in which sectioning images of confocal microscopy are used. Our experiment shows that uniformly magnified true 3-D image of micro-objects can be optically displayed in space using II. Our method can assist physicians, biologists, scientists, and engineers to perceive 3-D structure of micro-objects more vividly and accurately. Also, we have shown experimentally that the viewing resolution improvement of 3-D II is strongly dependent on the moving direction and travel distance of the lenslet array in the MALT. The results can be used to obtain the optimal parameters of moving lenslets for improved viewing resolution of 3-D II.

## References

- [1] S. A. Benton, ed., *Selected Papers on Three-Dimensional Displays* (SPIE Optical Engineering Press, Bellingham, WA, 2001).
- [2] D. H. McMahon, H. J. Caulfield, A technique for producing wide-angle holographic displays, *Appl. Opt.*, vol. 9, no. 1, 91-96, 1970.
- [3] T. Okoshi, Three-dimensional display, *Proc. IEEE*, vol. 68, 548-564, 1980.
- [4] G. Lippmann, La photographie integrale, *C. R. Acad. Sci.*, vol. 146, 446-451, 1908.
- [5] H. E. Ives, Optical properties of a Lippmann lenticulated sheet, *J. Opt. Soc. Am.*, vol. 21, 171-176, 1931.
- [6] C. B. Burckhardt, Optimum parameters and resolution limitation of integral photography, *J. Opt. Soc. Am.*, vol. 58, 71-76, 1968.
- [7] F. Okano, H. Hoshino, J. Arai, and I. Yuyama, Real-time pickup method for a three-dimensional image based on integral photography, *Appl. Opt.*, vol. 36, no. 7, 1598-1603, 1997.
- [8] F. Okano, H. Hoshino, J. Arai, and I. Yuyama, Three-dimensional video system based on integral photography, *Opt. Eng.*, vol. 38, no. 6, 1072-1077, 1999.
- [9] H. Hoshino, F. Okano, H. Isono, and I. Yuyama, Analysis of resolution limitation of integral photography, *J. Opt. Soc. Am. A*, vol. 15, no. 8, 2059-2065, 1998.
- [10] J.-H. Park, S.-W. Min, S. Jung, and B. Lee, Analysis of viewing parameters for two display methods based on integral photography, *Appl. Opt.*, vol. 40, no. 8, 5217-5232, 2001.
- [11] J.-S. Jang, F. Jin, and B. Javidi, Three-dimensional integral imaging with large depth of focus using real and virtual image fields, *Opt. Lett.*, vol. 28, no. 16, 1421-1423, 2003.
- [12] J.-S. Jang and B. Javidi, Improved viewing resolution of three-dimensional integral imaging with nonstationary micro-optics, *Opt. Lett.*, vol. 27, no. 5, 324-326, 2002.
- [13] S.-H. Shin and B. Javidi, Speckle-reduced three-dimensional volume holographic display by use of integral imaging, *Appl. Opt.*, vol. 41, no. 14, 2644-2649, 2002.

- [14] J.-S. Jang and B. Javidi, Improvement of viewing angle in integral imaging by use of moving lenslet arrays with low fill factor, *Appl. Opt.*, vol. 42, no. 11, 1996-2002, 2003.
- [15] S. Jung, J.-H. Park, H. Choi, and B. Lee, Wide-viewing integral three-dimensional imaging by use of orthogonal polarization switching, *Appl. Opt.*, vol. 42, no. 14, 2513-2520, 2003.
- [16] B. Lee, S. Y. Jung, S.-W. Min and J.-H. Park, Three-dimensional display by use of integral photography with dynamically variable image planes, *Opt. Lett.*, vol. 26, no. 19, 1481-1482, 2001.
- [17] J.-S. Jang and B. Javidi, Large depth-of-focus time multiplexed three-dimensional integral imaging using lenslets with non-uniform focal lengths and aperture sizes, *Opt. Lett.*, vol. 28, no. 20, 1924-1926, 2003.
- [18] J. W. Lichtman, Confocal microscopy, *Sci. Am.*, vol. 271, 30-35, 1994.
- [19] T. Wilson, ed. *Confocal Microscopy* (Academic Press, London, 1990).
- [20] K. Itoh, A. Hayashi, and Y. Ichioka, Digitized optical microscopy with extended depth of field, *Appl. Opt.*, vol. 28, 3487-3492, 1989.
- [21] M. Martinez-Corral, C. Ibáñez-López, and G. Saavedra, Axial gain resolution in optical sectioning fluorescence microscopy by shaded-ring filters, *Optics Express*, vol. 11, 1740-14745, 2003.
- [22] Born, M. & Wolf, E. *Principles of Optics*, 6<sup>th</sup> ed. (Pergamon Press, Oxford, 1980) 152-153.
- [23] J.-S. Jang and B. Javidi, Formation of orthoscopic three-dimensional real images in direct pickup one-step integral imaging, *Opt. Eng.*, vol. 42, no. 7, 1869-1870, 2003.
- [24] Y. Igarishi, H. Murata, and M. Ueda, 3D display system using a computer-generated integral photograph, *Japanese J. Appl. Phys.*, vol. 17, 1683-1684, 1978.
- [25] P. Ambs, L. Bigue, Y. Fainman, R. Binet, J. Colineau, J.-C. Leheureau, and J.-P. Huignard, Image reconstruction using electrooptic holography, *Proc. the 16<sup>th</sup> Annual Meeting of the IEEE Lasers and Electro-Optics Society*, vol. 1 (IEEE, Piscataway, N.J., 2003) 179-180.
- [26] <http://science.csustan.edu/confocal/Images/Animation/index.htm>.
- [27] J.-S. Jang and B. Javidi, Three-dimensional integral imaging with electronically synthesized lenslet arrays, *Opt. Lett.*, vol. 27, no. 20, 1767-1769, 2002.



## 감사의 글

제가 석사학위를 받는 과정에 많은 도움을 주셨던 분들을 위해 감사의 마음을 전하고자 합니다. 우선 저의 정신적인 아버지이셨던 고장주석 교수님께 가장 큰 고마움을 느낍니다. 생전에 저에게 연구에 대한 조언과 질타를 아낌없이 해 주셨고 또한, 어려운 가정 형편을 많이 도와 주셨습니다. 대학과 대학원 생활을 함에 있어 정신적인 지주 역할을 해 주셨습니다. 현재 이 세상에 계시지는 않지만, 앞으로 교수님의 연구 정신을 받들어 교수님의 이름을 빛낼 수 있는 제자가 되도록 하겠습니다.

저의 논문 완성을 지도해 주신 정신일 교수님, 김성운 교수님, 하덕호 교수님께 깊은 감사를 드립니다. 특히, 저의 지도교수님이신 하덕호 교수님의 많은 지도에 진심으로 감사를 드립니다. 또한, 연구에 많은 배려를 해 주신 박규철 교수님께도 진심으로 감사를 드립니다.

대학원 생활을 함에 있어, 연구 방법에 대해 많은 조언을 해주고 연구 내용에 대해 열띤 토론을 함께 해 준 연구실 선배 신동학 박사님, 중국 길림대학교 부교수로 재직 중이신 김복수 박사님, 그리고 연구실 생활을 많이 도와준 오용석 선배님께 고마움을 전합니다. 또한, 석사과정 동안, 저와 함께 연구를 도와준 후배 송용욱, 최동욱, 손유진에게 감사의 말을 전하고 싶습니다.

장주석 교수님의 유고집 편찬에 많은 힘을 써 주시고, 제가 무사히 석사과정을 마칠 수 있게 많은 도움을 주신 광운대학교 김은수 교수님에게 깊은 감사를 드립니다.

저의 7년 벗이고 제가 힘들 때 옆에서 위로 해 주고 모든 일에 있어 많은 조언을 해준 저의 영원한 친구 한재규에게 고맙다는 말을 전하고 싶습니다. 그리고, 옆에서 대학원 생활을 즐겁게 할 수 있도록 도와준 후배 황진호에게 감사드립니다. 또한, 대학 선배, 동기, 후배 모두에게 감사하는 마음을 전합니다.

마지막으로 어려운 가정형편으로 저에게 뒷바라지를 못해 준 것을 안타까워하셨던 부모님이시지만, 끝까지 아들을 믿고 이해해 주신 부모님께 이 영광을 돌리고자 합니다.